

pH-induced conformational changes of lupin protein-pectin mixtures and its effect on air-water interfacial properties and foaming functionality

Xingfa Ma, Mehdi Habibi, Leonard M.C. Sagis*

Laboratory of Physics and Physical Chemistry of Foods, Wageningen University, Bornse Weilanden 9, 6708 WG, Wageningen, the Netherlands

ARTICLE INFO

Keywords:

Lupin protein
Pectin
Co-soluble mixtures
Electrostatic complexes
Interfacial rheology
Lissajous plots
General stress decomposition
Interfacial structure
Foaming properties

ABSTRACT

Lupin protein isolate (LPI) has high nutritional value and good foaming properties around neutral pH; however, its functionality becomes poor at acidic pH, due to reduced protein solubility. The addition of pectin to LPI can increase its solubility at acidic pH and hence improve protein functionality. Here, we investigated the air-water interfacial and foaming properties of LPI-pectin (1:1) mixtures at pH 3.5–7.0. We used interfacial shear and dilatational rheology, characterized the air-water interfacial microstructure with AFM of Langmuir-Blodgett films, and linked the results to the foaming properties of the LPI-pectin mixtures. Based on the phase diagram, LPI and pectin formed co-soluble mixtures at pH 6.0 and 7.0, while LPI-pectin electrostatic complexes were formed at pH 3.5 and 4.0. In the co-soluble mixtures, proteins diffused faster towards the air-water interface than the electrostatic complexes, due to smaller particle sizes of the proteins. Their air-water interfaces showed distinct differences with respect to microstructure and mechanical properties. The interfaces stabilized by co-soluble mixtures were dominated by protein aggregates, leading to weaker interfaces in response to shear and dilatational deformation, while the complexes formed thicker and denser polymeric air-water interfaces that were stiffer and more solid-like. As a result, the complex-stabilized foams were more stable than those stabilized with co-soluble mixtures. Findings from this study indicate that soluble LPI-pectin complexes formed at pH 3.5 and 4.0 were more efficient in improving interfacial and foaming properties of LPI than the co-soluble mixtures at pH 6.0 and 7.0, which can be used to tailor the properties of acid aerated products stabilized by LPI.

1. Introduction

Currently, the protein transition from animal proteins to plant proteins enjoys increasing attention in the food industry, due to the health and environmental benefits of plant proteins (Blonk, Kool, Luske, De Waart, & ten Pierick, E., 2008; Floret, Monnet, Micard, Walrand, & Michon, 2023; Khandpur, Martinez-Steele, & Sun, 2021). Pulse proteins, such as peas, lentils, cowpeas, chickpeas, and lupins, are the most widely used protein sources in food formulations (Boye, Zare, & Pletch, 2010; Shevkani, Singh, Chen, Kaur, & Yu, 2019). Among these pulse proteins, lupin proteins are a promising protein source, due to their high nutritional value and good functionality (Lo, Kasapis, & Farahnaky, 2020; Pozani, Doxastakis, & Kiosseoglou, 2002). Comprehensive studies have shown four major types of protein in lupin protein extracts, namely α -, β -, γ -, and δ -conglutin (Klupait & Juodeikien, 2015; Rodríguez-Ambriz, Martínez-Ayala, Millán, & Davila-Ortiz, 2005; Salmanowicz & Weder, 1997; Shrestha, van't Hag, Haritos, & Dhital, 2021). The α -conglutin (11S) exists as a hexamer with a molecular weight ranging from 57.8 to

67.4 kDa and the monomers consist of a disulfide-bonded acidic and basic chain (Cabello-Hurtado et al., 2016; Foley et al., 2011). The β -conglutin (7S) is a trimer that lacks disulfide bonds to link its monomer units and has a molecular weight ranging from 68 to 75 kDa (Duranti, Consonni, Magni, Sessa, & Scarafoni, 2008; Foley et al., 2011). The δ -conglutin (2S) is a monomeric protein composed of two disulfide-bonded subunits with a molecular weight of 10.7–17.8 kDa (Duranti et al., 2008; Foley et al., 2011). Unlike the above proteins, the protein configurations of γ -conglutin (7S) vary with different pH. At pH 4.5, γ -conglutin exists as monomers due to the dissociation of their tetrameric structures. At a pH value larger than 5.5, γ -conglutin exhibits oligomeric structures consisting of dimer, tetramer, and cyclic hexamer (Mane, Johnson, Duranti, Pareek, & Utikar, 2018).

Lupin proteins have shown promising functionality at neutral pH with respect to foaming properties (Raymundo, Empis, & Sousa, 1998; Sathe, Deshpande, & Salunkhe, 1982), emulsifying properties (Burgos-Díaz et al., 2016; Chappleau & de Lamballerie-Anton, 2003), and gelling properties (Al-Ali et al., 2021; Berghout, Boom, & Van der Goot,

* Corresponding author.

E-mail address: leonard.sagis@wur.nl (L.M.C. Sagis).

<https://doi.org/10.1016/j.foodhyd.2024.110567>

Received 13 June 2024; Received in revised form 30 July 2024; Accepted 22 August 2024

Available online 27 August 2024

0268-005X/© 2024 The Authors. Published by Elsevier Ltd. This is an open access article under the CC BY license (<http://creativecommons.org/licenses/by/4.0/>).

2015). In the food industry, many protein beverages are produced in acidic conditions (Cosson, Souchon, Richard, Descamps, & Saint-Eve, 2020; Goudarzi, Madadlou, Mousavi, & Emam-Djomeh, 2015), however, the functionality of lupin is dramatically reduced at these pH ranges due to the decreased solubility at acidic pH values.

To improve the solubility of lupin protein at acidic pH, the mixing of proteins with polysaccharides is a frequently adapted method. Upon mixing proteins with polysaccharides, repulsive segregation or attractive association may occur depending on the charge of the proteins and polysaccharides, which may lead to the formation of co-soluble mixtures, phase separation, formation of soluble complexes, or insoluble complex coacervates (McClements, 2006). The phase diagram of protein-polysaccharide mixtures is often elucidated by measuring turbidity. Co-solubilization of protein and polysaccharides often occurs at high pH, when both protein and polysaccharide are negatively charged, leading to clear solutions. When the pH is stepwise decreased, soluble complexes start to form at a critical pH (denoted as pH_c) and the turbidity of the solutions starts to increase. With the further reduction of pH to $pH_{\phi 1}$, the turbidity of the solutions often shows a rapid increase, indicating the formation of insoluble coacervates. As the pH values are reduced further to pH_{opt} , complex coacervates reach their maximum yield, where the charges of coacervates are assumed to be neutral. Dissolutions of the complex coacervates occur at an even lower pH (denoted as $pH_{\phi 2}$), due to the protonation of polysaccharides at extremely low pH values (Klassen & Nickerson, 2012; Stone, Cheung, Chang, & Nickerson, 2013; J. Zhang et al., 2023).

In the past few years, the phase behavior of protein-polysaccharide mixtures as a function of pH, ionic strength, and total concentrations were extensively reported in many studies (Aryee & Nickerson, 2012, 2014; Bekale, Agudelo, & Tajmir-Riahi, 2015; Kaushik, Dowling, Barrow, & Adhikari, 2015; Liu, Low, & Nickerson, 2009; Sarraf, Naji-Tabasi, & Beig-babaei, 2021; Q. Zhang, Dong, Gao, Chen, & Vasanthan, 2020). There are several studies reporting the air-water interfacial properties of whey protein-polysaccharide mixed systems at pH 7.0 (Perez, Carrara, Sánchez, Santiago, & Patino, 2009; Perez, Carrara, Sánchez, Santiago, & Rodríguez Patino, 2010), soy protein-polysaccharide mixtures at pH 7.0 (Martinez, Sanchez, Ruiz-Henestrosa, Patino, & Pilosof, 2007), and lysozyme/ovalbumin-pectin complexes at pH 3.5 (Humblet-Hua, van der Linden, & Sagis, 2013). The functionality of protein-polysaccharide mixtures was also previously studied with respect to emulsifying properties (Girard, Turgeon, & Paquin, 2002; Kato, Sato, & Kobayashi, 1989; Tian et al., 2020) and foaming properties (Jarpa-Parra, Tian, Temelli, Zeng, & Chen, 2016; Makri, Papalamprou, & Doxastakis, 2005; Xu et al., 2020). But there is still a lack of understanding of the interfacial properties of protein-polysaccharides mixtures in different phase states (co-soluble mixtures vs. soluble complexes) and how differences in interfacial properties between these two states affect foaming properties.

In a previous study (Ma, Habibi, & Sagis, 2024), we showed that the soluble fraction of LPI at pH 3.5 and 4.0 had better foaming properties than those at pH 7.0 and 6.0. But protein solubility was severely reduced at pH 3.5 and 4.0, which makes application of LPI at such a pH nonviable from an economic and sustainability perspective. To improve protein solubility and further improve foaming functionality at acidic pH, we therefore mixed LPI with pectin at pH 3.5–7.0 to study their interfacial and foaming properties. In this study, we first investigated the phase behavior of lupin protein-pectin mixtures (1:1 ratio) in a pH range from 1 to 7. Subsequently, we compared the air-water interfacial properties (interfacial adsorption behavior, interfacial shear and dilatational rheology, and interfacial microstructure) of co-soluble mixtures (pH 6–7) to those of soluble complexes (pH 3.5–4.0). Finally, the interfacial properties were linked to the foaming properties of the systems. Findings from this study provide a comprehensive understanding of air-water interfacial properties and foam stabilization of lupin protein-pectin mixtures in different phase states, which could promote their

application in acid-aerated protein-based products.

2. Materials and methods

2.1. Materials

Lupin seeds were purchased from Kamelur (Germany), and all other chemicals were obtained from Sigma-Aldrich (USA). All solutions in this study were prepared in MiliQ water unless stated otherwise.

2.2. Extraction of lupin protein

The extraction of lupin protein isolates (LPI) was according to our previous method (Ma, Shen, Habibi, & Sagis, 2024). Briefly, the dehulling process of lupin seeds was performed by a laboratory-scale dehuller (Satake Corporation, Japan). Afterward, the dehulled seeds were milled to full-fat lupin flour by a multimill (Hosokawa-Alpine, Augsburg, Germany), followed by defatting the full-fat flour with hexane at a 1:10 flour to hexane ratio (w/v) and repeating this process three times. Subsequently, the defatted flour was dispersed in MiliQ water before adjusting pH to 9.0, and then centrifuging the dispersion at 36,000 g for 10 min to collect the supernatant that contained proteins. The pH of the supernatant was adjusted to 4.6, and then allowing 90 min to precipitate proteins. The mixtures were centrifuged at 36,000 g for 5 min to collect precipitates. The precipitates were then redispersed in MiliQ water, followed by adjusting pH to 7.2 using 1M HCl. Lastly, the redispersed solutions were dialyzed over 12 kDa cut-off membranes against MiliQ water at 4 °C for 72 h before freeze drying. The resultant protein content of the LPI was $81.7 \pm 3.8\%$, based on a conversion factor of 5.7.

2.3. Purification of pectin

Low methoxyl pectin power (GENU®, 45CS) (CP Kelco (Atlanta, GA)) (degree of esterification of 38%) was initially dispersed in MiliQ water to a concentration of 1 wt% and then dialyzed over 12 kDa cut-off membranes against distilled water at 4 °C for 72 h before freeze drying.

2.4. Preparation of sample solutions

Lupin protein solutions and pectin solutions were dispersed in MiliQ water to a concentration of 0.2 wt%, followed by stirring for 4 h and left overnight to allow for protein/pectin hydration. The mixed solutions were prepared by initially mixing lupin protein solutions and pectin solutions at a 1:1 ratio, and subsequently diluting the mixtures with 40 mM pH 7.0 phosphate buffer, 40 mM pH 6.0 phosphate buffer, 40 mM pH 4.0 acetate buffer, and 40 mM pH 3.5 citrate buffer to obtain a total biopolymer concentration of 0.1 wt% in corresponding 20 mM buffer. Similarly, 0.2 wt% of the mixed LPI-pectin solutions were prepared by mixing 0.4 wt% LPI solutions and 0.4 wt% pectin solutions, followed by diluting the mixed solutions with 40 mM corresponding buffer at a 1:1 ratio (v/v).

2.5. Turbidimetric analysis of LPI-pectin mixtures

The turbidity of LPI-pectin mixtures was measured at pH values ranging from 1 to 7 using a visible light spectrophotometer (Lambda 265, PerkinElmer, USA) at 600 nm. The pH of LPI-pectin mixtures was adjusted by 1 M NaOH or 0.1, 0.5, and 1 M HCl aqueous solutions. The transmittance (%) of the mixtures was immediately measured after pH adjustment. The turbidity (%) of the mixtures was calculated as $100 - \text{transmittance} (\%)$. The protein and pectin solutions were used as controls.

2.6. Determination of particle size and zeta potential

The particle size and zeta potential of 0.1 wt% LPI-pectin mixtures at pH 7, pH 6, pH 4, and pH 3.5 were measured by dynamic light scattering in a Zetasizer Nano ZS (Malvern Instruments, UK). All samples were prepared in a 20 mM buffer (phosphate, acetate, or citrate). The refractive index of the dispersed and continuous phase was set at 1.45 and 1.33, respectively. The zeta potential was calculated using the Smoluchowski model (F(ka) value of 1.5). All measurements were performed in triplicates at 25 °C.

2.7. Morphology of lupin protein-pectin mixtures

Samples were prepared by depositing 5 μ l 0.01% of LPI-pectin mixtures on a freshly cleaved mica sheet and subsequently dried in a desiccator for two days. Afterward, an atomic force microscope (AFM, NanoWizard® 4XP NanoScience, Bruker Nano GmbH, Germany) fitted with a PEAKFORCE-HIRS-F-A cantilever (spring constant of 0.42 N/m and a normal tip radius of 1 nm) was used to image the morphology of LPI-pectin mixtures. The systems were operated in a peak force tapping mode and the scan area was set at $10 \times 10 \mu\text{m}^2$ and $2 \times 2 \mu\text{m}^2$ with a line rate of 1.7 Hz and setpoint of 0.5 nN. The data were analyzed using the Nanoscope Analysis v1.5 software (Bruker, USA).

2.8. Interfacial adsorption behavior

The interfacial adsorption behavior of LPI-pectin mixtures at the air-water interface at different pH was monitored by a bubble pressure tensiometer (BPT) and an automatic drop tensiometer (ADT) within sub-second and long-time regimes, respectively. Regarding the BPT measurement, 15 ml of samples were injected into a glass container, followed by a continuous monitoring of surface tension from 10 ms to 30,000 ms. For the ADT measurement, a rising air droplet of 15 mm^2 was generated at the tip of a G16 needle and subsequently equilibrated for 3 h. The surface tension was continuously calculated by the built-in software, based on fitting the shape of the droplet with the Young-Laplace equation. The surface pressure (Π) was calculated as $\Pi(t) = \gamma_0 - \gamma(t)$, where γ_0 is the surface tension of the clean air-water interface and $\gamma(t)$ is the surface tension in real-time.

2.9. Interfacial shear rheology

The interfacial properties in shear deformation were measured by an AR G2 rheometer (TA Instruments, USA) coupled with a double wall ring (DWR) geometry. Briefly, the DWR geometry was positioned at the air-water interface and subsequently pre-sheared for 5 min, after which the interface was allowed to equilibrate for 3 h, before further performing frequency and amplitude sweeps. The frequency sweeps were performed by increasing frequency from 0.01 to 10 Hz at a fixed strain of 1%, while the strain sweeps were conducted at strains ranging from 0.01 to 100% at a fixed frequency of 0.1 Hz. All experiments were performed in triplicate at 20 °C.

2.10. Interfacial dilatational rheology

The interfacial dilatational rheology of LPI-pectin mixed solutions at different pH was measured with an ADT. A rising bubble was initially generated at the tip of a G16 needle and subsequently equilibrated for 3 h before further being subjected to frequency or amplitude sweeps. The frequency sweep was conducted at frequencies from 0.005 to 0.1 Hz and a fixed strain of 3%, while the amplitude sweep was performed at strains from 3% to 50% and a fixed frequency of 0.02 Hz. Five cycles were conducted for both frequency and amplitude sweeps with 50s rest time between each set of five cycles. All experiments were performed at least in triplicate at 20 °C.

2.11. Interfacial thickness

The interfacial thickness of the air-water interface stabilized by LPI-pectin mixtures was measured by an imaging nulling ellipsometer EP4 (Accurion, Germany). Briefly, 15 ml of the sample was transferred into a Petri dish (60 mm in diameter), and subsequently equilibrated for 3 h. The thickness of the air-water interfaces was then measured by an incident-polarized laser light beam in the wavelength range from 499.8 nm to 793.8 nm. Since the involvement of phase shift (δ) causes large errors in the model fitting, only the amplitude ratio (Ψ) from the data was analyzed with the EP4Model v.3.6.1. software, with the Cauchy model, assuming refractive indexes of 1.45, 1.45, 1.36, and 1.40, for the LPI-pectin mixtures at pH 7.0, pH 6.0, pH 4.0, and pH 3.5, respectively, to fit the thickness of the interface.

2.12. Preparation of Langmuir-Blodgett films and AFM imaging

Langmuir-Blodgett (LB) films of LPI-pectin mixtures at the air-water interfaces were prepared by a Langmuir trough (KSV NIMA/Biolin Scientific Oy, Finland). Briefly, the trough was filled with buffer (pH 3.5–7) and then a freshly cleaved mica sheet (Highest Grade V1 Mica, Ted Pella, USA) was immersed in the buffer. Subsequently, 1 ml of sample was injected at the bottom of the trough and then the interface was left to equilibrate for 3 h. Afterward, the Teflon barriers moved at a speed of 5 mm/min to compress the air-water interface until reaching a surface pressure of 10 mN/m or 20 mN/m. Next, the mica sheet was withdrawn at a speed of 1 mm/min, while keeping the surface pressure constant by moving the Teflon barriers. Duplicate films were prepared for each sample.

Imaging of these LB films was performed by AFM and followed the same procedures as in Section 2.7. These AFM images were further quantitatively analyzed using the Angiotool 64 software (National cancer Institute, National Institute of Health, Maryland, USA). Briefly, vessel area, vessel percentage area, junction density, average vessel length, end-point rate, branching rate, and mean lacunarity were calculated to characterize the structures observed in the images (Bernklau, Lucas, Jekle, & Becker, 2016; Munialo, van der Linden, Ako, & de Jongh, 2015).

2.13. Foaming properties of LPI-pectin mixtures

Foamability and foam stability of LPI-pectin mixtures at different pH were determined by whipping and gas sparging methods, respectively. For the foamability measurement, 15 ml of 0.1 wt% and 0.2 wt% samples were transferred into a plastic cylinder and subsequently whipped at 2000 rpm for 2 min using an overhead frother (Aerolatte Ltd., United Kingdom). The foamability was expressed as overrun, and calculated as overrun (%) = foam volume (ml)/initial liquid volume (ml) \times 100%. For the foam stability measurement, 40 ml of 0.1 wt% and 0.2 wt% samples were transferred into a glass cylinder ($\phi = 25 \text{ mm}$), followed by sparging N_2 gas from the bottom of the cylinder at a gas flow rate of 180 mL/min to a foam volume of 60 cm^3 . The time required for half of the volume of foam to decay, the so-called half-life time, was used to evaluate the foam stability. The bubble size of the foam was measured by squeezing 4 ml of freshly formed foam between two transparent Plexiglas plates ($10 \times 10 \text{ cm}$) with a fixed gap of 0.26 mm. The 2D morphology (Figs. S3 and S5) of air bubbles was captured by a high-resolution camera and was subsequently analyzed by ImageJ to calculate the bubble size distribution (Figs. S4 and S6).

2.14. Statistical analysis

One-way analysis of variance (ANOVA) of the data was conducted by OriginPro 2021. The means comparison among samples was conducted by Tukey's test using a significant level of 0.05.

3. Results and discussion

3.1. Physicochemical properties of lupin protein-pectin mixtures

The turbidity of LPI, LPI-pectin mixtures (1:1 ratio), and pectin in the pH range from 1.0 to 7.0 is shown in Fig. 1A. The turbidity of pectin solutions was almost constant at all pH values, suggesting it is soluble in this pH range. In contrast, LPI solutions showed extremely high turbidity (almost 100%) at pH values close to its pI, indicating protein aggregation. When further lowering the pH, the LPI solutions became less turbid again due to the increased net positive charges of LPI, which allowed the protein to partially resolubilize. The turbidity curve of LPI-pectin mixtures was similar to that of LPI, but their critical pH transition values (pH_C , $pH_{\phi 1}$, pH_{opt} , and $pH_{\phi 2}$) were shifted to lower pH values. When decreasing the pH to 6.0 (pH_C), the turbidity remained almost constant, implying the co-solubility of LPI and pectin in solutions. As the pH was reduced to 3.5 ($pH_{\phi 1}$), the turbidity of LPI-pectin mixtures was slightly increased, suggesting the formation of soluble complexes due to the enhanced electrostatic interactions between LPI and pectin in a more acidic environment. Below $pH_{\phi 1}$, the turbidity of LPI-pectin mixed solutions dramatically increased, and reached its maximum at 2.5 (pH_{opt}), indicating the formation of complex coacervates. When further reducing the pH to 1.5 ($pH_{\phi 2}$), the acidification of solutions caused the disassociation of insoluble LPI-pectin coacervates due to the protonation of carboxyl groups of pectin (J. Zhang et al., 2023), resulting in a reduction of overall turbidity.

As illustrated in Fig. 1B, for LPI-pectin mixtures, the zeta potential gradually increased when reducing the pH from 7.0 to 3.5, from about -40 mV to roughly -20 mV. The particle size distributions of LPI-pectin mixtures at different pH are shown in Fig. 1C. The mixed solutions at all pH displayed a bimodal distribution, where the first peak was smaller than 100 nm, while the second peak was around 197.6–311 nm. For pH 6.0 and 7.0, the first peak may correspond to individual proteins or small protein aggregates (e.g., dimers, trimers, etc.), and the second peak we assume are larger protein clusters dispersed in the bulk solution. At pH 4.0, both the primary and secondary peaks shifted to the right, and at pH 3.5, the first peak is no longer visible, and the distribution is monomodal, with a maximum at 311 nm. Apparently, at pH 4.0 the solution contains both protein clusters (~ 59.1 nm) and soluble complexes (~ 267.2 nm), whereas at 3.5 the sample contains mostly complexes (some unbound protein monomers should be present, but the scattering is dominated by the larger complexes, and monomers are therefore not visible in the distribution).

To confirm the DLS data, AFM imaging was used to visualize the

complex morphology at different pH values, as illustrated in Fig. 2. At pH 7.0 and 6.0, some fibrous and globular aggregates were visible, up to several hundred nm in size, which co-existed and were well separated from each other. These most likely correspond to chains of pectin and lupin protein aggregates, respectively. At pH 4.0 and 3.5, large and dense clusters (around 100–300 nm) were formed with protruding chain structures. These observations suggest LPI and pectin were co-solubilized in solution at pH 7.0 and 6.0 due to the strong electrostatic repulsions between biopolymers, while LPI-pectin complexes were formed at pH 4.0 and 3.5 due to the dominance of attractive interactions over repulsive forces. It is important to mention that the overall composition of the LPI-pectin mixtures at different pH values was not significantly different. We prepared LPI-pectin mixtures by first preparing LPI and pectin solutions in MilliQ water. Subsequently, we mixed LPI and pectin solutions at a 1:1 ratio and then diluted the blends in the appropriate buffer to make LPI-pectin mixtures at different pH values. In this way, we could avoid precipitation of protein due to its low solubility at acidic pH, which would certainly have affected the interfacial and foaming properties of the mixtures. Our protocol retains both LPI and pectin in solution (or dispersed, when complexes are formed) over the entire tested pH range. As a result, any differences we observe in their interfacial and foaming properties, should be mostly induced by their mutual interactions, and hence by the differences in the structures they form (i.e. co-soluble mixtures versus complexes).

3.2. Adsorption behaviors of lupin protein-pectin mixtures towards air-water interface

The interfacial adsorption behavior of lupin protein-pectin mixtures at pH 7.0 (LPI-pectin-7), 6.0 (LPI-pectin-6), 4.0 (LPI-pectin-4), and 3.5 (LPI-pectin-3.5) were studied by BPT (Fig. 3A) and ADT (Fig. 3B), within the sub-second (0.7–30 s) and long-time (1–10800 s) regimes, respectively.

To investigate the early-stage adsorption mechanism of LPI-pectin mixtures to the air-water interface (diffusion-controlled versus energy barrier-controlled), we rescaled the adsorption curves shown in Fig. 3A to obtain a single master curve, by dividing by a shifting factor to obtain a normalized time scale (Fig. S1A). We further plotted the shifting factor (the adsorption lag time) against particle size (from Fig. 1A) in Fig. S1B. The power law relationship between particle size and adsorption lag time ($d \sim t^n$) showed an n value of 2.3, which was much higher than the ideal diffusion-controlled process with an n value of 0.5, implying the adsorption is not purely diffusion-controlled. The adsorption of LPI-pectin mixtures may still be affected by energy barriers (e.g.,

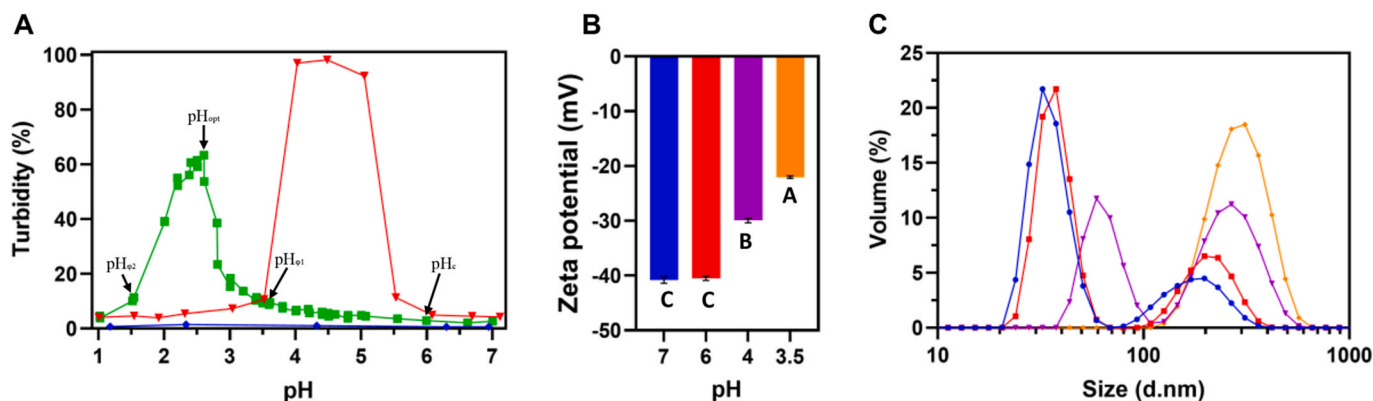


Fig. 1. (A) Turbidity curve of lupin protein (\blacktriangle), LPI-pectin mixtures (\blacksquare), and pectin (\blacklozenge) as a function of pH (1.0–7.0). (B) Zeta potential of lupin protein-pectin mixtures at pH 7.0, 6.0, 4.0, and 3.5. (C) The volume-based particle size distribution of 0.1 wt% lupin protein-pectin mixtures at pH 7.0 (\bullet), pH 6.0 (\blacksquare), pH 4.0 (\blacktriangle), and pH 3.5 (\blacklozenge). One-way ANOVA with Tukey's test was used to test the significance levels among samples, and different letters (A–C) represent significant differences ($p < 0.05$).

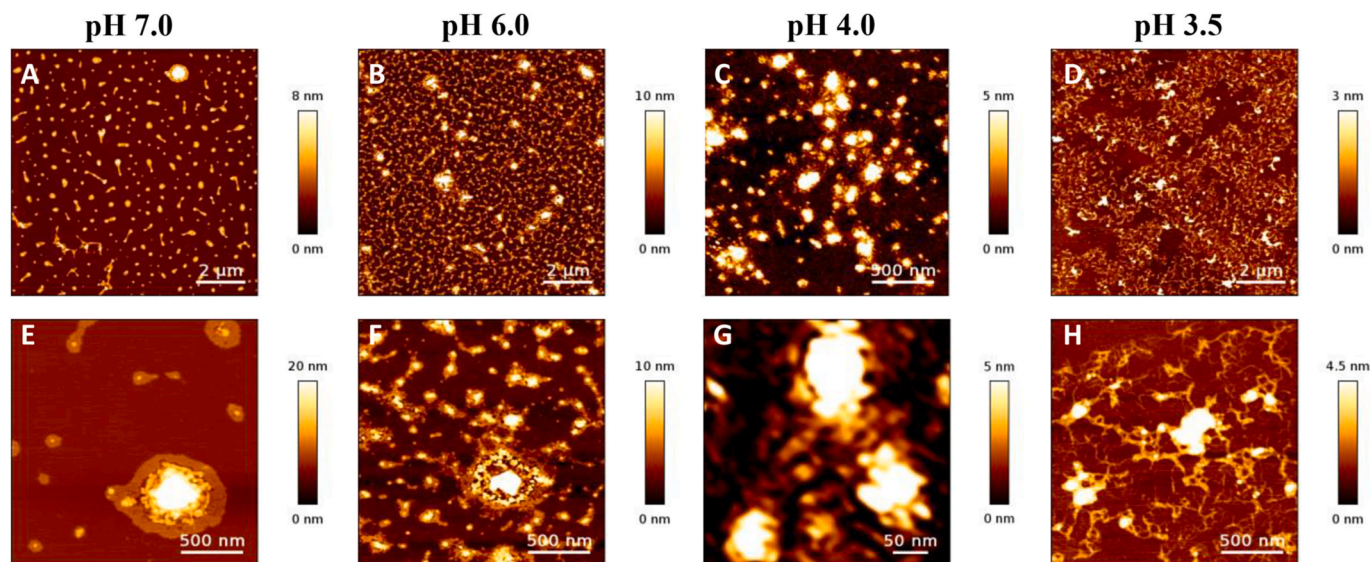


Fig. 2. The morphology of LPI-pectin mixtures, imaged with AFM, at pH 7.0 (A–E), pH 6.0 (B–F), pH 4.0 (C–G), and pH 3.5 (D–H).

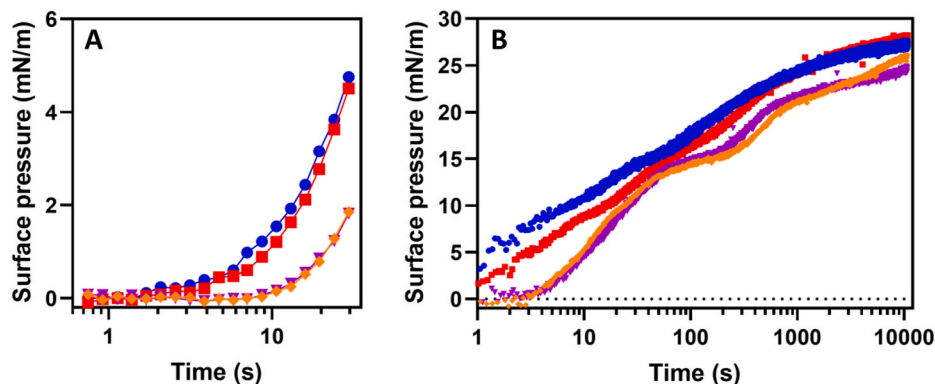


Fig. 3. Surface pressure of 0.1 wt% LPI-pectin mixtures as a function of time at pH 7.0 (●), pH 6.0 (■), pH 4.0 (▼), and pH 3.5 (◆), measured by (A) bubble pressure tensiometer (BPT) in the short-time regime (0.7 s–30s) and (B) automatic drop tensiometer, in the long-time regime up to 10,800 s. For a comparison of these results to the data for pure LPI at pH 3.5–7.0, the reader is referred to (Ma, Habibi, & Sagis, 2024).

electrostatic repulsion) that slow down their rate of adsorption to the interface. At pH 7.0 and 6.0, LPI and pectin were co-soluble in the bulk phase, and the adsorption of LPI-pectin mixtures to the interface was mainly dominated by LPI, and pectin will most likely remain in the bulk phase. Compared with pure LPI at pH 7.0 and 6.0, the addition of pectin dramatically reduced the rate of adsorption of proteins to the air-water interface and resulted in a longer adsorption lag time (as shown in Fig. S1D). This may be caused by the higher viscosity of the LPI-pectin mixtures. For LPI-pectin complexes at pH 4.0 and 3.5, LPI-pectin-3.5 had a slightly larger particle size than LPI-pectin-4 (as shown in Fig. 1C), however, these two complexes ended up with a comparable adsorption lag time of 3.3 ± 0.3 s. This could be explained by their difference in zeta potential as shown in Fig. 2B. LPI-pectin-3.5 was less negatively charged (-22.0 ± 0.2 mV) than LPI-pectin-4 (-29.9 ± 0.4 mV), resulting in a reduced electrostatic repulsion between LPI-pectin-3.5 and the negatively charged air-water interface (Beattie, Djerdjev, & Warr, 2009; Li & Somasundaran, 1991; Manciu & Ruckenstein, 2012; Takahashi, 2005), that may offset the adsorption delay induced by its larger particle size.

For the long-term adsorption behaviors (from 1 to 10,800 s) as shown in Fig. 3B, the co-soluble mixtures at pH 7.0 and pH 6.0 reached a surface pressure of 27.6 mN/m and 28.2 mN/m, respectively, after 3-h adsorption, while the complexes at pH 4.0 and pH 3.5 reached a relatively lower surface pressure of 24.7 mN/m and 25.8 mN/m,

respectively. This difference in surface pressure between co-soluble mixtures and electrostatic complexes might be caused by differences in the interfacial microstructure. In the next section, we will further investigate the mechanical properties by measuring the interfacial shear and dilatational rheology and imaging the air-water interfacial structure with AFM.

3.3. Interfacial shear rheology of lupin protein-pectin mixture stabilized interfaces

3.3.1. Frequency sweeps

After 3 h adsorption, the LPI-pectin mixture stabilized interfaces were subjected to oscillatory shear deformations in frequency sweeps. As shown in Fig. 4A, all interfaces showed a larger value for G' than for G'' in the applied frequency range, indicating a predominantly solid-like viscoelastic behavior for the air-water interfaces. The change of G' as a function of frequency was fitted with a power law model ($G' \sim \omega^n$), and the n values (Fig. 4B) of all interfaces were between 0.12 and 0.16, suggesting the formation of disordered solid interfacial structures, similar to what was observed for whey proteins (Yang, Thielen, Berton-Carabin, van der Linden, & Sagis, 2020). The deviation from the power law dependence observed above 3 Hz is most likely the effect of inertial forces. The power law fit was hence applied only to frequencies < 3 Hz.

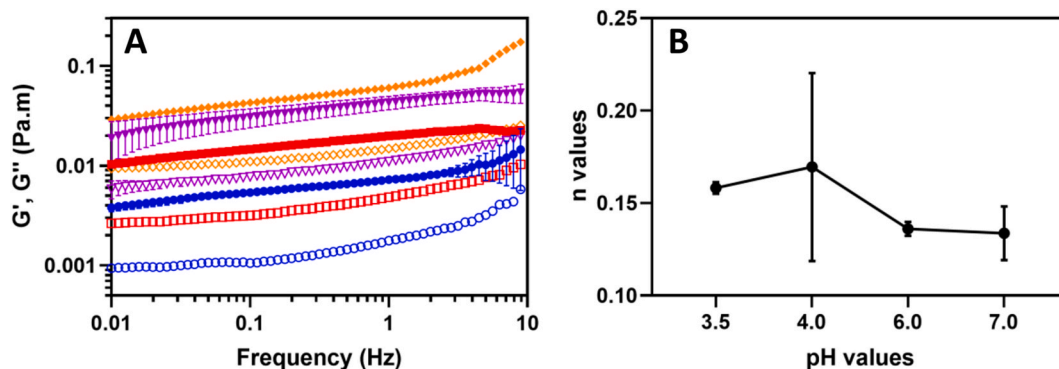


Fig. 4. (A) Interfacial shear modulus (G' and G'') of LPI-pectin mixtures at pH 7.0 (● and ○), pH 6.0 (■ and □), pH 4.0 (▼ and ▽), and pH 3.5 (◆ and ◇), as a function of frequency (0.01–10 Hz) and at a fixed strain of 1%. (B) The power law fitting exponent n calculated from the interfacial shear frequency sweep at 1% strain for LPI-pectin mixtures at pH from 3.5 to 7.0.

3.3.2. Strain sweeps

Fig. 5A illustrates the strain sweeps of LPI-pectin mixtures at different pH, which showed constant G' and G'' values until a critical strain (9% for LPI-pectin-7, 5% for LPI-pectin-6, 2% for LPI-pectin-4 and LPI-pectin-3.5), which represents the extent of the linear viscoelastic (LVE) regime. In the LVE regimes, all interfaces again showed $G' > G''$, indicating solid-like interfaces, where the complex (LPI-pectin-4 and LPI-pectin-3.5) stabilized interfaces had higher G' values than the co-soluble mixture (LPI-pectin-7 and LPI-pectin-6) stabilized interfaces, suggesting that the electrostatic complexes formed stiffer air-water

interfaces. Additionally, the co-soluble mixtures showed longer LVE regimes than the complexes, suggesting the co-soluble mixtures formed weaker but more stretchable interfaces. In the non-linear viscoelastic (NLVE) regimes, the G' and G'' values started to decrease until a critical cross-over point, where the value of G' drops below the value of G'' , which indicates the air-water interfaces transitioned from solid-like to liquid-like behavior. The co-soluble mixtures had a cross-over point beyond 100%, while the complexes (LPI-pectin-4 and LPI-pectin-3.5) had a cross-over point of 25%. These results suggest that the complex stabilized interfaces were severely disrupted in the applied strain range,

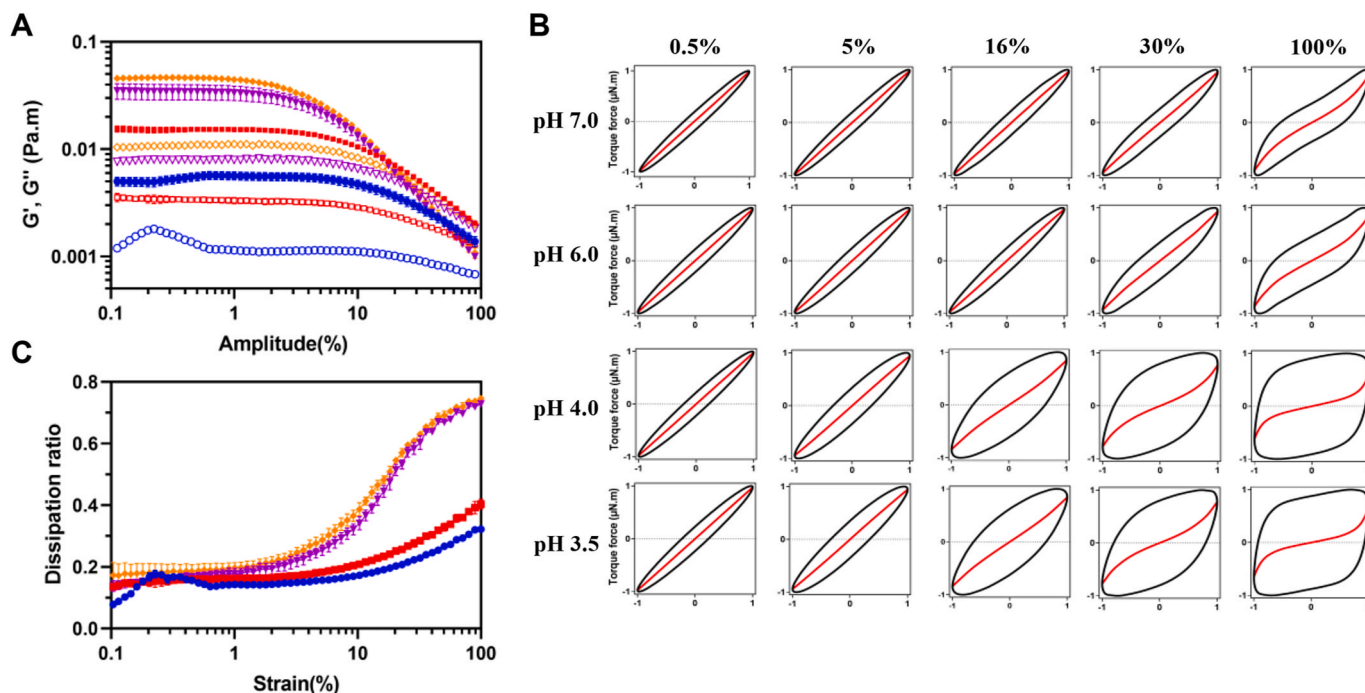


Fig. 5. (A) Interfacial shear modulus (G' and G'') of LPI-pectin mixture at pH 7.0 (● and ○), pH 6.0 (■ and □), pH 4.0 (▼ and ▽), and pH 3.5 (◆ and ◇) as a function of strain (0.1–100%) and at a fixed frequency of 0.1 Hz. (B) Normalized Lissajous plots of torque vs. strain of lupin protein-pectin mixtures at pH 7.0, pH 6.0, pH 4.0, and pH 3.5. The loop represents the total torque, while the red line inside the loop represents the elastic contributions to the total torque. (C) The dissipation ratio as a function of the strain of lupin protein-pectin mixture stabilized interfaces at pH 7.0 (—●—), pH 6.0 (—■—), pH 4.0 (—▼—), and pH 3.5 (—◆—).

while the interfacial structures of co-soluble mixtures remained relatively more intact in the NLVE regime.

To get more insight into the linear and non-linear behaviors of LPI-pectin mixed interfaces at different pH, normalized Lissajous plots were constructed (Fig. 5B). In the LVE regimes (0.5%), all plots had a narrow ellipse shape with straight decomposed elastic curves, suggesting the predominance of elastic behavior. In the NLVE regimes, all Lissajous plots became rhomboidal and wider with inverted sigmoidal decomposed elastic curves, indicating partial disruption of the interfacial microstructure and an increased viscous contribution to the total stress. For the LPI-pectin-7 and LPI-pectin-6 stabilized interfaces, their Lissajous plots are barely distorted at 30% strain and show a significant elastic behavior even at 100% strain. These results suggest an almost intact interfacial structure for LPI-pectin-7 and LPI-pectin-6, even under larger shear deformations. In contrast, LPI-pectin-4 and LPI-pectin-3.5 showed a clear transition to plastic behavior at 100% strain, with nearly zero slope of the decomposed elastic curves, which suggests the interfacial structures of these interfaces were mostly disrupted under large deformation. The energy dissipation ratio ($\Phi = \pi G'' \gamma_0 / 4 \sigma_{\max}$, where G'' is the loss modulus, γ_0 is the strain amplitude, and σ_{\max} is the maximum stress) was also calculated to quantitatively characterize the viscoelastic behaviors of these Lissajous plots in the LVE and NLVE regimes (Fig. 5C). Within the LVE regime, all interfaces showed Φ values below 0.2, indicating the dominance of elasticity in the LVE regime. When the strains increased towards the NLVE regime, the Φ values of LPI-pectin-7 and LPI-pectin-6 slowly increased to 0.3 and 0.4 at 100%, respectively, indicating still predominantly elastic behavior at large deformations. In contrast, the Φ values of LPI-pectin-4 and LPI-pectin-3.5 increased relatively fast and reached values higher than 0.7 at 100% strain, close to $\pi/4$ (the value for a Newtonian fluid). This suggests that these interfaces behaved like Newtonian films at large shear deformations and thus exhibited mostly viscous behavior due to the disruption of interfacial microstructures.

Overall, LPI-pectin co-soluble mixtures at pH 7 and 6 form a less stiff air-water interface in response to small shear deformations than the electrostatic complexes at pH 4 and 3.5. However, the co-soluble mixture interfaces are more stretchable and resistive in response to large shear deformation than those stabilized by the complexes.

3.4. Interfacial dilatational rheology of lupin protein-pectin stabilized interfaces

3.4.1. Frequency and amplitude sweeps

The air-water interfaces stabilized with LPI-pectin mixtures at different pH were studied by conducting dilatational frequency and amplitude sweeps in a drop tensiometer. In the frequency sweeps (Fig. 6A), all interfaces showed power-law behavior ($E_d' \sim \omega^n$) with n

values significantly smaller than 0.5. This indicates the low exchangeability of these interfacial stabilizers between bulk and interfaces (Lucassen & Van Den Tempel, 1972), and together with $E_d' \gg E_d''$ implied the formation of disordered soft solid-like interfaces.

In the amplitude sweeps (Fig. 6B), the elastic modulus (E_d') of LPI-pectin-4 and LPI-pectin-3.5 dramatically decreased by a factor of 2–4, upon increasing amplitude from 3% to 50%, indicating the disruption of interfacial structures by the increased deformation. In contrast, LPI-pectin-7 and LPI-pectin-6 showed slightly lower reductions in E_d' by only a factor of 0.5–1 with amplitudes increased to 50%. The E_d' of LPI-pectin-7 and LPI-pectin-6 were significantly lower at 5% than that of LPI-pectin-4, and LPI-pectin-3.5. These observations suggest the LPI-pectin co-soluble mixtures at pH 7 and 6 form less stiff air-water interfaces in response to small dilatational deformations, but they were more stretchable and less disrupted at large deformations, compared with the complexes at pH 4 and 3.5. This is in accordance with the observations in the interfacial shear experiments. To analyze the dilatational data more accurately, Lissajous curves were constructed. These are discussed in the next section.

3.4.2. Lissajous plots of interfacial dilatational rheology

To further analyze the viscoelastic behaviors of LPI-pectin mixture stabilized air-water interfaces in the small and large deformations regime, Lissajous plots (surface pressure vs. deformation) were constructed, as shown in Fig. 7. The Lissajous plots are characterized by a closed loop in a clockwise direction with applied deformation, where the extension and compression of the interface are represented by the upper and lower parts of the plot, respectively.

At 5% amplitude, all plots, especially LPI-7 and LPI-6, were ellipsoidal and narrow, indicating predominantly elastic behaviors. The LPI-pectin-4 and LPI-pectin-3.5 stabilized interfaces had a steeper slope of these plots than LPI-7 and LPI-6, indicating higher interfacial stiffness at small deformations. With amplitudes increased to 30% and 50%, the Lissajous plots became wider and asymmetric. The strain-softening upon extension is a result of the disruption of interfacial structure and reduction of the interfacial density, and the strain-hardening upon compression is most likely resulting from the jamming of the interfacial structure. At both 30% and 50% amplitudes, LPI-pectin-4 and LPI-pectin-3.5 clearly showed a wider loop than LPI-pectin-6 and LPI-pectin-7, indicating that the total mechanical response of LPI-pectin-4 and LPI-pectin-3.5 stabilized air-water interfaces at large deformations had more contributions from network disruption and density change. In the next section, we will further use the general stress decomposition (de Groot, Yang, & Sagis, 2023) to separate these two responses.

3.4.3. General stress decomposition

The quantitative analysis of the nonlinearities at large deformation

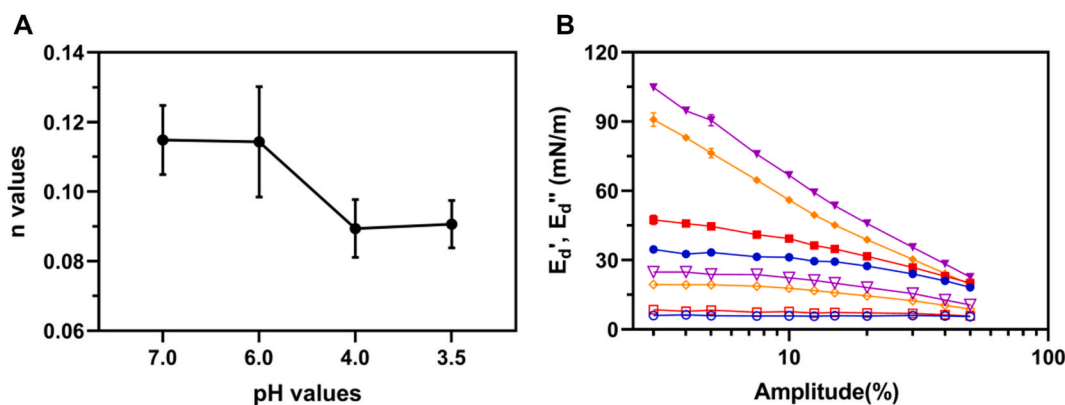


Fig. 6. (A) The n values calculated from fitting power-law models to the data of the interfacial dilatational frequency sweeps at a fixed strain of 3% for the LPI-pectin mixtures at pH 7.0, pH 6.0, pH 4.0, and pH 3.5. (B) Interfacial dilatational elastic modulus (E_d') and viscous modulus (E_d'') as a function of amplitude and at a fixed frequency of 0.02 Hz for LPI-pectin mixtures at pH 7.0 (—●—), pH 6.0 (—■—), pH 4.0 (—▼—), and pH 3.5 (—◆—).

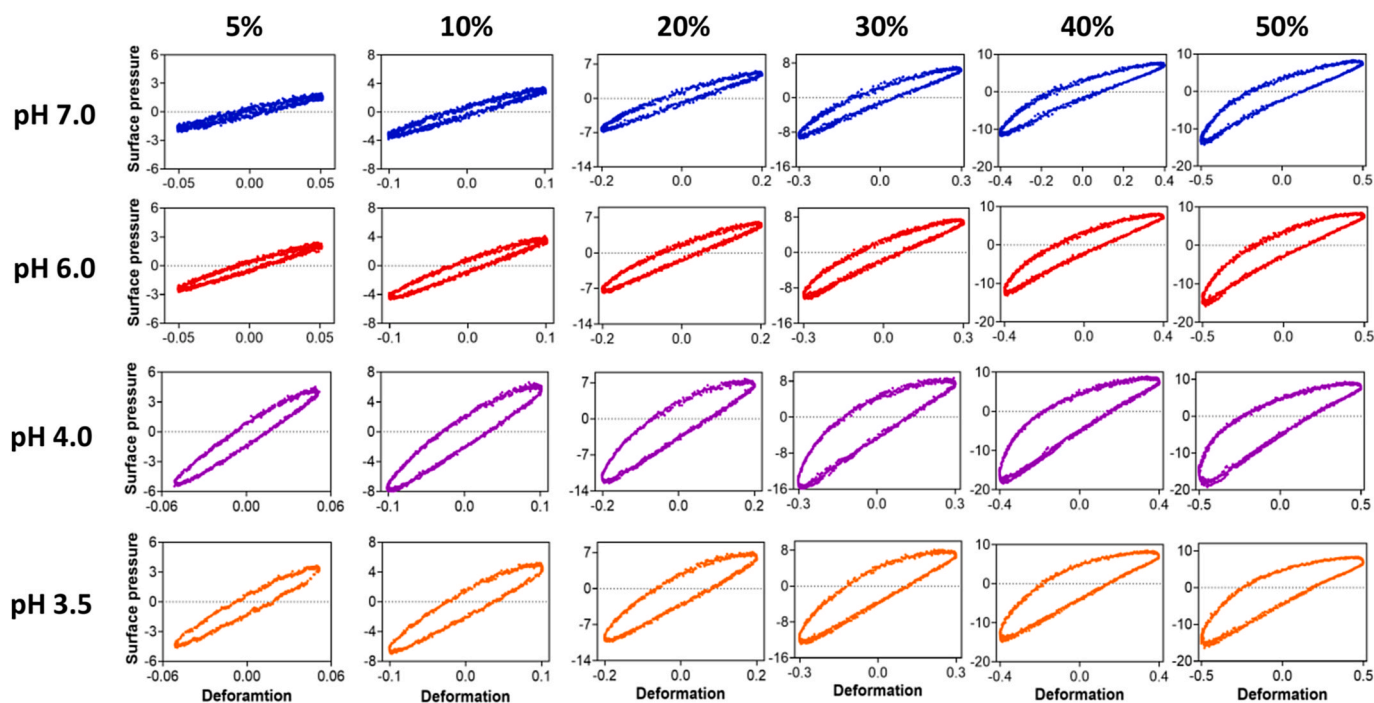


Fig. 7. Lissajous plots of surface pressure as a function of deformation for LPI-pectin mixtures at pH 7.0 (●), pH 6.0 (■), pH 4.0 (▼), and pH 3.5 (◆) and at 5–50% amplitude. For clarity, only one plot is shown for each amplitude, but all triplicate results are comparable.

was conducted using the general stress decomposition, where the total stress responses were decomposed based on the odd and even harmonics of the total stress signals. Here, the odd harmonics represent the network disruption of the interface, which can be split into elastic (τ_1) and viscous (τ_2) contributions. The even harmonics describe the interfacial density change during dilatational oscillation and constitute dissipative (τ_3) and elastic (τ_4) contributions (detailed explanations of these parameters can be found in de Groot et al. (2023)).

The secant modulus ($E_{\tau_{1L}}$), the slope of the curve connecting the origin with the value of τ_1 at maximum intra-cycle strain, indicates the stiffness of the air-water interface. As shown in Fig. 9 A, all interfaces clearly illustrated a decreasing trend for $E_{\tau_{1L}}$ with increasing amplitude, suggesting the disruption of the interfacial structure at large deformation. LPI-pectin-4 and LPI-pectin-3.5 stabilized interfaces showed a significantly higher $E_{\tau_{1L}}$ modulus than LPI-pectin-7 and LPI-pectin-6 at small deformation, indicating the complex stabilized interfaces were stiffer than the co-soluble ones. The $E_{\tau_{1L}}$ for LPI-pectin-7 and LPI-pectin-6 showed only small reductions with increased amplitude. This indicates that LPI-pectin-7 and LPI-pectin-6 formed weaker but more stretchable interfaces, which was in line with the shear rheology experiments, where these samples had the lowest G' in the LVE regime but retained relatively more elastic behavior in the NLVE regime. The viscous contributions of the odd harmonics (τ_2) and even harmonics (τ_3) were represented by a closed spherical loop (Fig. 8B) and a lemniscate shape (Fig. 8C), respectively, and their total area was calculated as dissipative energy ($U_{d\tau_2}$) due to network disruption (Fig. 9D) and dissipative energy ($U_{d\tau_3}$) due to surface density changes, respectively. At 50% amplitude, the LPI-pectin-4 stabilized interfaces showed a wider closed loop and higher $U_{d\tau_2}$ and $U_{d\tau_3}$ values than other interfaces, indicating stronger in-plane interactions. In line with the previous results, LPI-pectin-7 and LPI-pectin-6 had the lowest values of $U_{d\tau_2}$ and $U_{d\tau_3}$, these samples formed much weaker air-water interfaces.

The elastic part of the even harmonics, τ_4 , was characterized by a single curve (Fig. 8D) and represents the energy storage from the surface pressure-area work exerted on the interfaces due to the changes in surface density. The extent of the τ_4 curves was quantitatively characterized by the E_{τ_4} modulus (as shown in Fig. 9B), again a secant modulus,

defined as the slope of the curve connecting the point in the τ_4 curve at zero strain to the point in the curve at maximum intra-cycle strain. Larger deformations (>10%) resulted in a more negative value of E_{τ_4} for LPI-pectin-4 compared to other interfaces (Fig. 9B), suggesting a more important role of surface density changes in the LPI-pectin-4 stabilized interfaces in the total stress response. The stress τ_4 is not centered around the horizontal axis and its vertical shift indicated by γ_s is given in Fig. 9C. This shift is a measure for how far the applied deformations are driving the system out of equilibrium. LPI-pectin-4 clearly had a more negative shift of τ_4 curves (i.e., more negative values of γ_s shown in Fig. 9C) at large deformations (50%) than LPI-pectin-7, LPI-pectin-6, and LPI-pectin-3.5, suggesting that oscillations are performed around a nonequilibrium state far from the equilibrium surface pressure-area isotherm. Based on the highly negative values of E_{τ_4} modulus and significantly negative shift of the τ_4 curve for LPI-pectin-4, we can conclude that LPI-pectin-4 may form a dense air-water interface that limits in-plane relaxation behavior, resulting in a slow restoring of the LPI-pectin-4 interfaces to equilibrium at zero intra-cycle deformation. The higher value of $U_{d\tau_3}$ for LPI-pectin-4 compared to other samples again indicates the formation of a denser interface for LPI-pectin-4 that caused more energy dissipations from the surface density changes at large deformations.

Overall, LPI-pectin-4 appears to form a more densely packed interfacial film with strong in-plane interactions that limit bulk-interface exchange. LPI-pectin-3.5 forms a slightly less stiff interface, but is still significantly stronger than LPI-pectin-6. LPI-pectin-7 displayed the lowest interfacial stiffness and lowest contributions of surface density changes to the total surface stress, indicating the formation of weak interfaces with weak in-plane interactions. To check the conclusions from the GSD, we prepared Langmuir-Blodgett films and then imaged them by AFM, and these are discussed in the next section.

3.5. Interfacial structure of LPI-pectin mixtures at different pH

To reveal the air-water interfacial structure of LPI-pectin mixtures at different pH, Langmuir-Blodgett (LB) films were prepared at 10 mN/m and 20 mN/m and then observed by AFM. The air-water interfacial

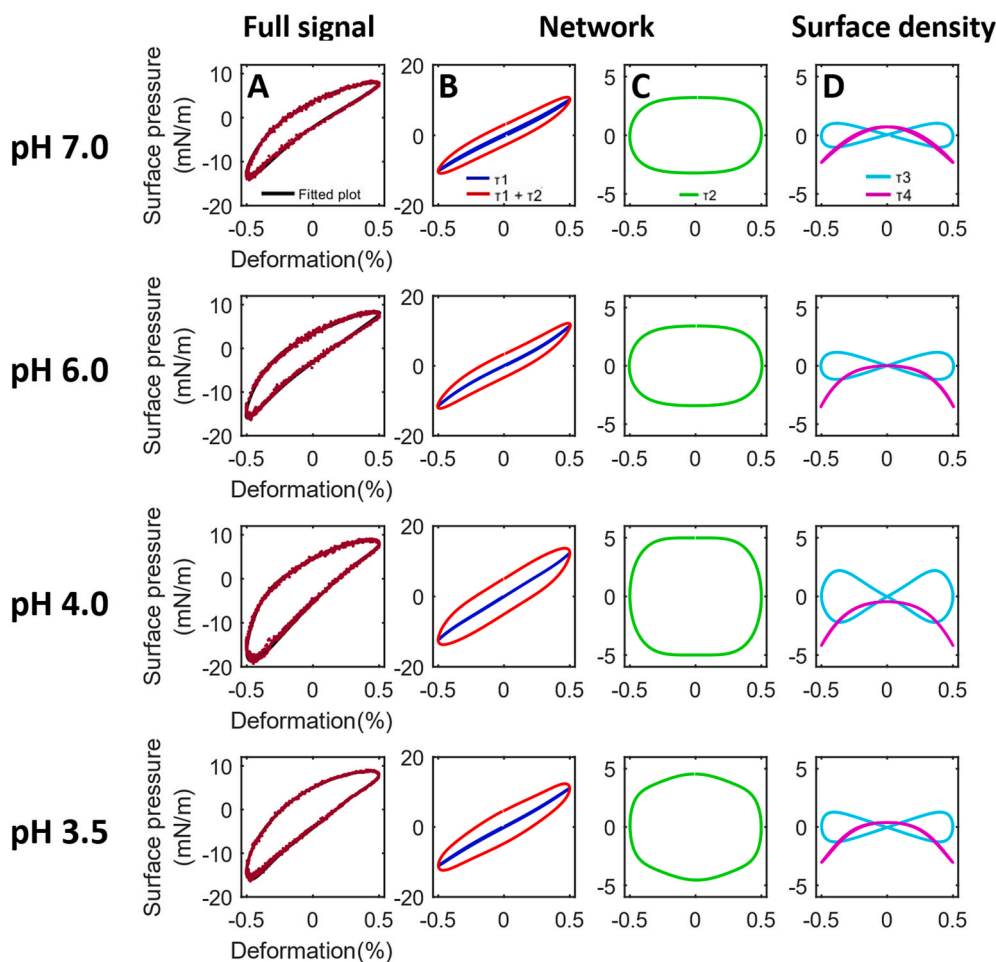


Fig. 8. Decomposed Lissajous plots of LPI-pectin mixtures at pH 7.0, pH 6.0, pH 5.0, pH 4.0, and pH 3.5, from top to bottom, at an amplitude of 50%. The fitted full signal is shown in black (—), τ_1 is shown in dark blue (—), $\tau_1 + \tau_2$ is shown in red (—), τ_2 is shown in green (—), τ_3 is shown in cyan (—), and τ_4 is shown in magenta (—).

thickness of LPI-pectin mixtures at pH from 3.5 to 7 was also measured with ellipsometry, which was then compared with the thickness of pure LPI at the same pH range (Fig. S7).

The pH adjustment of the LPI and pectin mixed solutions showed a significant change to the interfacial microstructure (Fig. 10). At the lower surface pressure of 10 mN/m, we observed a clear transition of an interfacial microstructure formed by aggregated protein at pH 6.0–7.0 to more polymeric interfaces at pH 3.5–4.0. The co-soluble mixtures at pH 6.0–7.0 showed comparable interfacial structures and thickness (Fig. S7) as pure LPI stabilized interfaces at pH 6.0–7.0 (Ma, Habibi, and Sagis (2024)), where protein clusters dominate the air-water interface. Based on this, it can be inferred that only protein molecules adsorbed at the air-water interfaces, while pectin molecules remained in the bulk phase. At pH 4.0 and 3.5, we observed a strikingly different air-water interface of these mixtures from pure LPI, where the complex stabilized interfaces consisted of long connected strands that surrounded large globular aggregates (Fig. 10D and E), while the pure LPI stabilized interfaces were composed of a more homogeneously distributed fine-stranded protein clusters (Ma, Habibi, and Sagis (2024)). The interfacial thickness of LPI-pectin mixtures at pH 4.0 and 3.5 was significantly higher than that of pure LPI at the same pH range, suggesting the presence of pectin molecules at the air-water interface. Overall, the complex stabilized air-water interfaces at pH 4.0 and 3.5 were dominated by polymeric structures and were significantly thicker than the protein-dominated interfaces at pH 7.0 and 6.0 (Fig. S7).

LB films were also prepared at a surface pressure of 20 mN/m, which is comparable to the surface pressure of the air-water interfaces in the

interfacial shear and dilatational rheology. To quantitatively analyze the network structure of these air-water interfaces, image analysis of these AFM images was conducted using the AngioTool 64 software. At a surface pressure of 20 mN/m, the mixtures at pH 4 and 3.5 showed more pronouncedly enhanced network formation with higher connectivity, longer network threads, a higher level of network branching, and a lower level of open-ended network threads than those at pH 7 and 6, as indicated by their higher network area, higher junction density, longer average vessel length, higher branching rates, lower end point rates, and lower lacunarity (Fig. 11A–F). LPI-pectin-7 formed an interface consisting of clustered proteins, with lower connectivity between the proteins, which explains the lower interfacial stiffness in response to shear and dilatational deformations compared to LPI-pectin-4 and LPI-pectin-3.5. The combination of a lower value of $E_{\tau_{1L}}$ with a weak dependence on strain amplitude for LPI-pectin-7, suggests LPI-pectin-7 formed a soft-glass-like or weak gel-like interfacial structure. As indicated from GSD results, the LPI-pectin-4 and LPI-pectin-3.5 stabilized interfaces had a strong contribution from odd harmonics ($E_{\tau_{1L}}$ and $U_{d\tau_2}$) in dilatation, suggesting the formation of strong 2d gel-like interfaces. The denser interfaces of LPI-pectin-4 (at a surface pressure of 20 mN/m) as indicated from image analysis, were in line with the higher contributions from even harmonics (E_{τ_4} and $U_{d\tau_3}$) for LPI-pectin-4 stabilized interfaces, compared to all other ones.

3.6. Foaming properties of LPI-pectin mixtures at different pH

The foamability and foam stability of 0.1 wt% and 0.2 wt% of LPI-

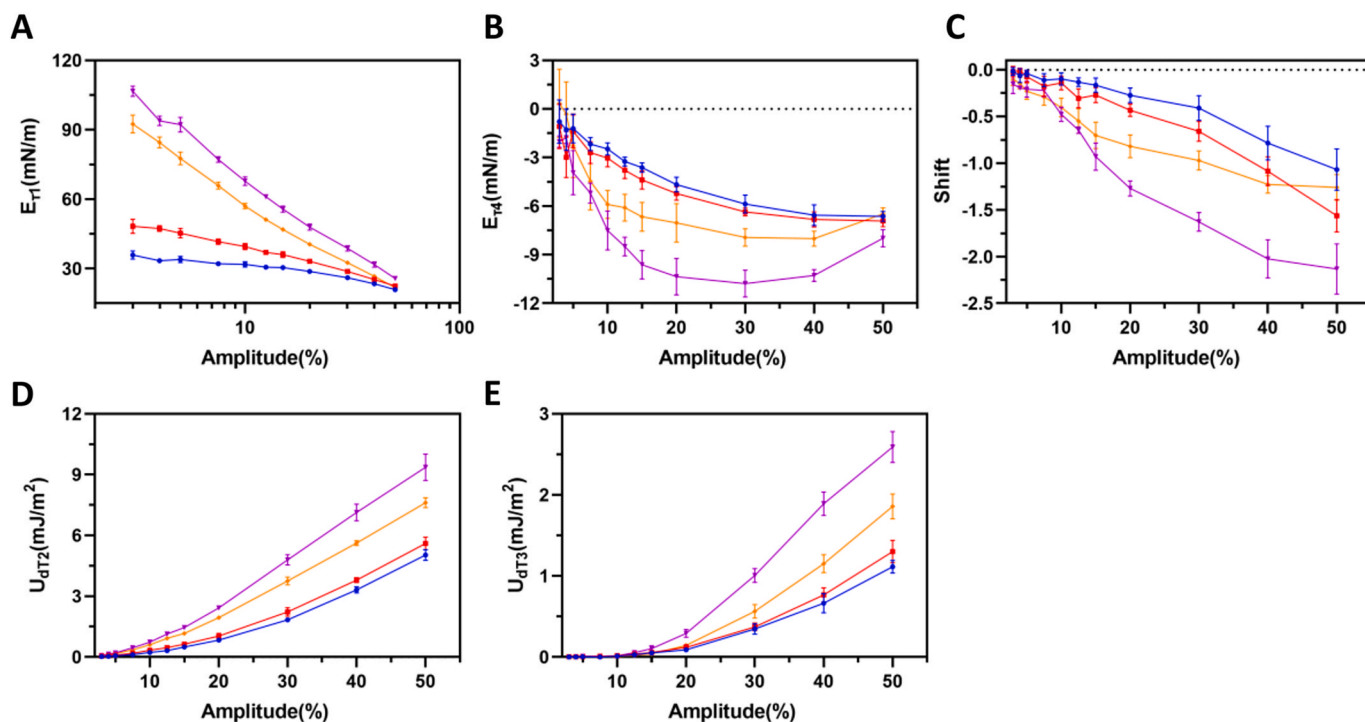


Fig. 9. The secant modulus of τ_1 (A), modulus of τ_4 (B), vertical shift (γ_s) of τ_4 (C), dissipated energy of τ_2 (D), dissipated energy of τ_3 (E) as a function of amplitude (%) for LPI-pectin mixtures at pH 7.0 (—●—), pH 6.0 (—■—), pH 4.0 (—▲—), and pH 3.5 (—◆—).

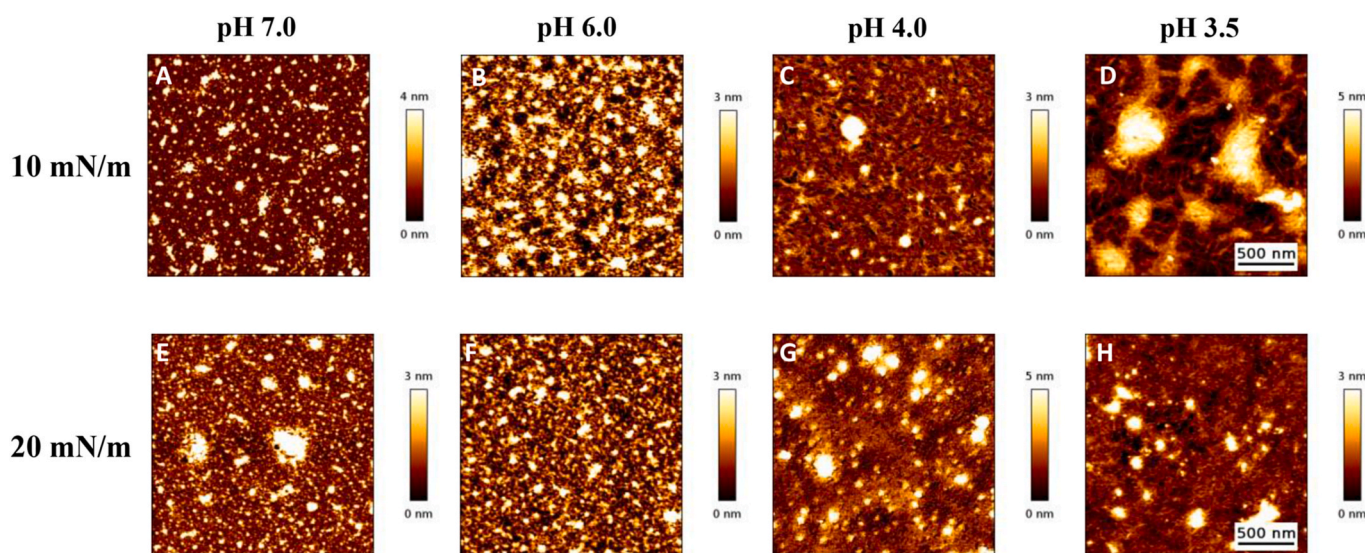


Fig. 10. AFM images of Langmuir-Blodgett films of LPI-pectin mixtures at pH 7.0 (A–E), pH 6.0 (B–F), pH 4.0 (C–G), and pH 3.5 (D–H). The surface pressure used for film preparation is 10 mN/m and 20 mN/m, and the measured relative height (color scale) is indicated on the right side.

pectin mixtures at pH 3.5–7 were measured by whipping and N₂ gas sparging and then compared to 0.1 wt% of soluble LPI at the same pH range. The foamability was characterized by overrun, while the foam stability was assessed by the foam half-life time, according to a previous study (Yang, Berton-Carabin, Nikiforidis, van der Linden, & Sagis, 2022).

At 0.1 wt% of total concentration, the foam overrun of mixtures did not change much when reducing the pH from 7.0 to 3.5 (Fig. 12A), and was significantly lower than pure soluble LPI. This may be the result of the lower protein content in the 1:1 LPI-pectin mixtures, which is only 0.05 wt%, leading to larger bubble sizes (Fig. 12C), and more coalescence during foam formation. As the total concentration increased to

0.2 wt%, the overrun of the mixtures at pH 4.0 and 3.5 dramatically increased from 86% to 98% respectively at 0.1 wt%, to 300% and 330% respectively at 0.2 wt% (Fig. 12A), and were now higher than the overrun of pure LPI at these pH values. The LPI-pectin complexes at pH 4.0 and 3.5, adsorbed slower to the air-water interface than pure LPI at pH 4.0 and 3.5. But the complexes formed stiffer air-water interfaces than the soluble LPI (Fig. S2). These two effects may offset to some extent, causing a slightly higher overrun for LPI-pectin mixtures at pH 4.0 and 3.5.

The overrun of the mixtures at pH 6.0–7.0 was only slightly increased at 0.2 wt%, and still significantly lower than the overrun of pure LPI, even though the protein content of the samples was now equal.

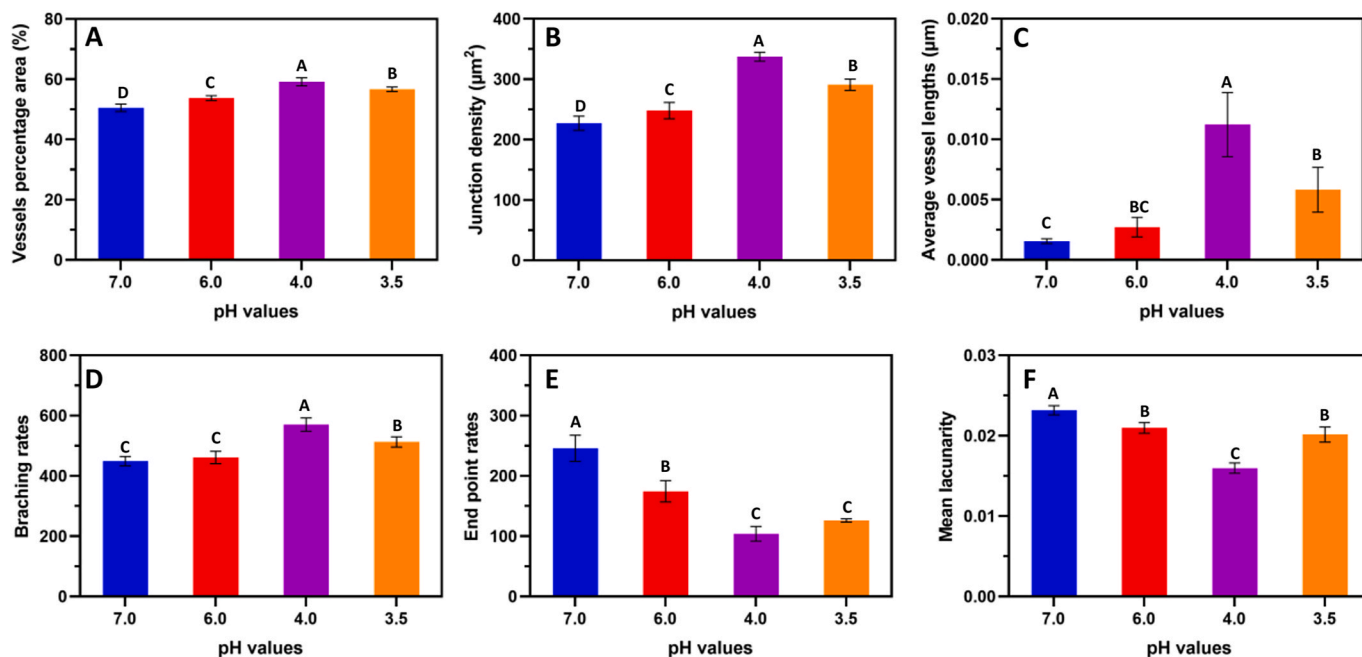


Fig. 11. Protein network analysis of AFM images at a surface pressure of 20 mN from Fig. 10 for LPI-pectin mixtures at pH 7.0, pH 6.0, pH 4.0, and pH 3.5. The parameters determined by AngioTool are shown in (A) vessel percentage area, (B) junction density, (C) average vessel length, (D) branching rates, and (E) endpoint rates. One-way ANOVA with Tukey's test was used to test the significant levels among samples, and different letters (A–D) represent significant differences ($p < 0.05$).

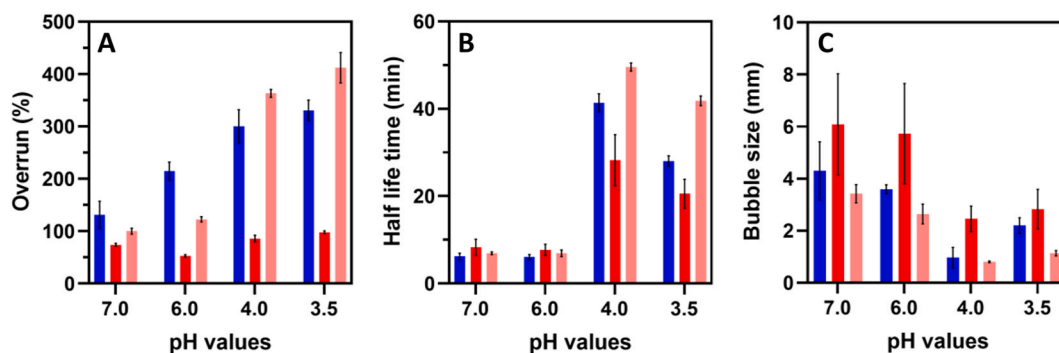


Fig. 12. Foaming properties (overrun (A), volume-based half-life time (B), and bubble size (C)) of 0.1 wt% (red) and 0.2 wt% (pink) LPI-pectin mixtures at pH 7.0, pH 6.0, pH 5.0, pH 4.0, and pH 3.5, and 0.1 wt% soluble LPI (blue) at pH 7.0, pH 6.0, pH 4.0, and pH 3.5.

As shown in Fig. S1, pure LPI at pH 7.0 and 6.0 clearly adsorbed faster at the air-water interface (i.e., had a lower adsorption lag time) than the LPI-pectin co-soluble mixtures at pH 7.0 and 6.0, which explains the significantly higher foaming overrun of LPI at these pH values. The higher overrun of the mixtures at pH 4.0 and 3.5 compared to those at pH 7.0 and 6.0 is most likely the result of the higher interfacial stiffness against shear and dilatational deformation, that reduced bubble coalescence after formation and resulted in smaller air bubbles (Fig. 12C).

At both 0.1 wt% and 0.2 wt% total concentration, the foam stability of the mixtures at pH 3.5–7.0 was ranked as follows according to their half-life time (Fig. 12B): pH 4.0 > pH 3.5 > pH 6.0 = pH 7.0, which was positively correlated to their interfacial dilutional modulus (at 5%) as shown in Fig. 6B. Similar results were reported by Xu et al. (2020), where soluble whey protein-sodium alginate complexes at pH 4.0 exhibited higher foam stability than the co-soluble mixtures at pH 7.0 (Xu et al., 2020). The higher interfacial stiffness of the LPI-pectin mixtures at pH 4.0 and 3.5 could explain their higher foam half-life time and stability. In comparison with the 0.1 wt% LPI at pH 4.0 and 3.5, the 0.2 wt% complexes showed slightly higher foam half-life time, while the half-life time of the 0.1 wt% LPI (at pH 7 and 6) and 0.2 wt% co-soluble

mixtures was not clearly different (Fig. 12B). These observations can be explained by the interfacial properties, where the complexes at pH 4.0 and 3.5 formed a stiffer air-water interface than LPI, while the interfacial stiffness of LPI and co-soluble mixtures was not significantly different at pH 7.0 and 6.0 (Fig. S2).

4. Conclusions

This study systematically explored the interfacial properties and foaming properties of lupin protein-pectin mixtures in different phase states (co-soluble mixtures versus soluble complexes), and their foaming properties were subsequently compared to lupin protein in the same pH range. At pH 7.0 and 6.0, LPI and pectin were co-soluble in the bulk phase, and the air-water interfaces were dominated by protein molecules, while pectin remained in the bulk solution. In comparison, at pH 4.0 and 3.5, complexes were formed due to attractive electrostatic interactions. These complexes adsorbed slower to the air-water interface due to the larger particle size of complexes and formed thicker and denser 2D gel-like interfacial structures that consisted of long connected strands that surrounded large aggregates, while the co-solubilized

mixtures adsorbed faster to the interface due to the smaller particle size of proteins but formed thinner and coarser interfacial layers with large protein clusters. These differences in interfacial structures between LPI-pectin co-soluble mixtures and electrostatic complexes resulted in significantly different interfacial mechanical properties in response to shear or dilatational rheology. The interfacial layers of LPI-pectin complexes at pH 4.0 and 3.5 were stiffer with stronger in-plane interactions than those of co-soluble mixtures at pH 7.0 and 6.0. The stiffer interfaces of LPI-pectin-4 and LPI-pectin-3.5 also resulted in higher foam stability than LPI-pectin-7 and LPI-pectin-6 at both 0.1 wt% and 0.2 wt% total biopolymer concentration.

Compared with LPI at pH 4.0 and 3.5, LPI-pectin-4 and LPI-pectin-3.5 form stiffer air-water interfaces with stronger in-plane interactions and higher interfacial thickness, while LPI-pectin-7 and LPI-pectin-6 showed comparable interfacial stiffness and thickness with LPI at pH 7.0 and 6.0. Consequently, the foams stabilized with 0.2 wt% LPI-pectin-4 and 0.2 wt% LPI-pectin-3.5 were more stable than 0.1 wt% LPI at pH 4.0 and 3.5, while the foam stability of 0.1 wt% LPI and 0.2 wt% LPI-pectin mixtures was not significantly different at pH 7.0 and 6.0.

Overall, lupin protein-pectin complexes at pH 4.0 and 3.5 showed better interfacial and foaming properties than the co-soluble mixtures at pH 7.0 and 6.0. The addition of 0.1 wt% pectin to 0.1 wt% LPI at pH 4.0 and 3.5 (i.e., 0.2 wt% of complexes) considerably improved the foaming properties of 0.1 wt% LPI, while the addition of 0.1 wt% pectin to 0.1 wt% LPI (0.2% co-soluble mixtures) at pH 7.0 and 6.0 shows comparable foaming properties with 0.1 wt% LPI. Considering the lower solubility of LPI at pH 4.0 and 3.5, the addition of pectin to LPI at these pH ranges could greatly increase protein solubility and also improve protein foaming functionality, which could promote their applications in the food industry. Although this study characterizes the air-water interfacial structure of LPI-pectin mixtures using AFM on Langmuir-Blodgett films, the molecular interactions between these biopolymers at the air-water interface are yet to be quantified. Future studies may consider using synchrotron scattering techniques and fluorescence micro-spectroscopy techniques to fill this gap.

CRedit authorship contribution statement

Xingfa Ma: Writing – review & editing, Writing – original draft, Visualization, Validation, Methodology, Investigation, Conceptualization. **Mehdi Habibi:** Writing – review & editing, Supervision, Methodology, Conceptualization. **Leonard M.C. Sagis:** Writing – review & editing, Supervision, Methodology, Conceptualization.

Declaration of competing interest

The authors have declared that no competing interest exists.

Data availability

Data will be made available on request.

Acknowledgements

X. Ma acknowledges the funding from China Scholarship Council (CSC NO. 202207940007).

Appendix A. Supplementary data

Supplementary data to this article can be found online at <https://doi.org/10.1016/j.foodhyd.2024.110567>.

References

Al-Ali, H. A., Shah, U., Hackett, M. J., Gulzar, M., Karakyriakos, E., & Johnson, S. K. (2021). Technological strategies to improve gelation properties of legume proteins

- with the focus on lupin. *Innovative Food Science & Emerging Technologies*, 68, Article 102634.
- Aryee, F. N., & Nickerson, M. T. (2012). Formation of electrostatic complexes involving mixtures of lentil protein isolates and gum Arabic polysaccharides. *Food Research International*, 48(2), 520–527.
- Aryee, F. N., & Nickerson, M. T. (2014). Effect of pH, biopolymer mixing ratio and salts on the formation and stability of electrostatic complexes formed within mixtures of lentil protein isolate and anionic polysaccharides (κ -carrageenan and gellan gum). *International Journal of Food Science and Technology*, 49(1), 65–71.
- Beattie, J. K., Djerdjev, A. M., & Warr, G. G. (2009). The surface of neat water is basic. *Faraday Discussions*, 141, 31–39.
- Bekale, L., Agudelo, D., & Tajmir-Riahi, H. (2015). Effect of polymer molecular weight on chitosan–protein interaction. *Colloids and Surfaces B: Biointerfaces*, 125, 309–317.
- Berghout, J., Boom, R., & Van der Goot, A. (2015). Understanding the differences in gelling properties between lupin protein isolate and soy protein isolate. *Food Hydrocolloids*, 43, 465–472.
- Bernklau, I., Lucas, L., Jekle, M., & Becker, T. (2016). Protein network analysis—a new approach for quantifying wheat dough microstructure. *Food Research International*, 89, 812–819.
- Blonk, H., Kool, A., Luske, B., De Waart, S., & ten Pierick, E. (2008). Environmental effects of protein-rich food products in The Netherlands: Consequences of animal protein substitutes. *Blonk Milieu Advies, Gouda (NL)*.
- Boye, J., Zare, F., & Pletch, A. (2010). Pulse proteins: Processing, characterization, functional properties and applications in food and feed. *Food Research International*, 43(2), 414–431.
- Burgos-Díaz, C., Piornos, J. A., Wandersleben, T., Ogura, T., Hernández, X., & Rubilar, M. (2016). Emulsifying and foaming properties of different protein fractions obtained from a novel lupin variety AluProt-CGNA®(Lupinus luteus). *Journal of Food Science*, 81(7), C1699–C1706.
- Cabello-Hurtado, F., Keller, J., Ley, J., Sanchez-Lucas, R., Jorrín-Novo, J. V., & Ainouche, A. (2016). Proteomics for exploiting diversity of lupin seed storage proteins and their use as nutraceuticals for health and welfare. *Journal of Proteomics*, 143, 57–68.
- Chapleau, N., & de Lamballerie-Anton, M. (2003). Improvement of emulsifying properties of lupin proteins by high pressure induced aggregation. *Food Hydrocolloids*, 17(3), 273–280.
- Cosson, A., Souchon, I., Richard, J., Descamps, N., & Saint-Eve, A. (2020). Using multiple sensory profiling methods to gain insight into temporal perceptions of pea protein-based formulated foods. *Foods*, 9(8), 969.
- de Groot, A., Yang, J., & Sagis, L. M. (2023). Surface stress decomposition in large amplitude oscillatory interfacial dilatation of complex interfaces. *Journal of Colloid and Interface Science*, 638, 569–581.
- Duranti, M., Consonni, A., Magni, C., Sessa, F., & Scarafoni, A. (2008). The major proteins of lupin seed: Characterisation and molecular properties for use as functional and nutraceutical ingredients. *Trends in Food Science & Technology*, 19(12), 624–633.
- Floret, C., Monnet, A.-F., Micard, V., Walrand, S., & Michon, C. (2023). Replacement of animal proteins in food: How to take advantage of nutritional and gelling properties of alternative protein sources. *Critical Reviews in Food Science and Nutrition*, 63(7), 920–946.
- Foley, R. C., Gao, L.-L., Spriggs, A., Soo, L. Y., Goggin, D. E., Smith, P. M., et al. (2011). Identification and characterisation of seed storage protein transcripts from *Lupinus angustifolius*. *BMC Plant Biology*, 11, 1–15.
- Girard, M., Turgeon, S., & Paquin, P. (2002). Emulsifying properties of whey protein-carboxymethylcellulose complexes. *Journal of Food Science*, 67(1), 113–119.
- Goudarzi, M., Madadlou, A., Mousavi, M. E., & Emam-Djomeh, Z. (2015). Formulation of apple juice beverages containing whey protein isolate or whey protein hydrolysate based on sensory and physicochemical analysis. *International Journal of Dairy Technology*, 68(1), 70–78.
- Humblett-Hua, N.-P. K., van der Linden, E., & Sagis, L. M. (2013). Surface rheological properties of liquid–liquid interfaces stabilized by protein fibrillar aggregates and protein–polysaccharide complexes. *Soft Matter*, 9(7), 2154–2165.
- Jarpa-Parra, M., Tian, Z., Temelli, F., Zeng, H., & Chen, L. (2016). Understanding the stability mechanisms of lentil legumin-like protein and polysaccharide foams. *Food Hydrocolloids*, 61, 903–913.
- Kato, A., Sato, T., & Kobayashi, K. (1989). Emulsifying properties of protein–polysaccharide complexes and hybrids. *Agricultural & Biological Chemistry*, 53(8), 2147–2152.
- Kaushik, P., Dowling, K., Barrow, C. J., & Adhikari, B. (2015). Complex coacervation between flaxseed protein isolate and flaxseed gum. *Food Research International*, 72, 91–97.
- Khandpur, N., Martinez-Steele, E., & Sun, Q. (2021). Plant-based meat and dairy substitutes as appropriate alternatives to animal-based products? *The Journal of Nutrition*, 151(1), 3–4.
- Klassen, D., & Nickerson, M. (2012). Effect of pH on the formation of electrostatic complexes within admixtures of partially purified pea proteins (legumin and vicilin) and gum Arabic polysaccharides. *Food Research International*, 46(1), 167–176.
- Klupait, D., & Juodeikien, G. (2015). Legume: COMPOSITION, protein extraction and functional properties. *A REVIEW. Chemine technologija*, (1).
- Li, C., & Somasundaran, P. (1991). Reversal of bubble charge in multivalent inorganic salt solutions—effect of magnesium. *Journal of Colloid and Interface Science*, 146(1), 215–218.
- Liu, S., Low, N. H., & Nickerson, M. T. (2009). Effect of pH, salt, and biopolymer ratio on the formation of pea protein isolate–gum Arabic complexes. *Journal of Agricultural and Food Chemistry*, 57(4), 1521–1526.

- Lo, B., Kasapis, S., & Farahnaky, A. (2020). Lupin protein: Isolation and techno-functional properties, a review. *Food Hydrocolloids*, 112(March 2021).
- Lucassen, J., & Van Den Tempel, M. (1972). Dynamic measurements of dilational properties of a liquid interface. *Chemical Engineering Science*, 27(6), 1283–1291.
- Ma, X., Habibi, M., & Sagis, L. M. (2024). Interfacial and foaming properties of soluble lupin protein isolates: Effect of pH. *Food Hydrocolloids*, Article 110228.
- Ma, X., Shen, P., Habibi, M., & Sagis, L. M. (2024). Interfacial properties and functionality of lupin protein-pectin complexes at the air-water interface. *Food Hydrocolloids*, 110050.
- Makri, E., Papalamprou, E., & Doxastakis, G. (2005). Study of functional properties of seed storage proteins from indigenous European legume crops (lupin, pea, broad bean) in admixture with polysaccharides. *Food Hydrocolloids*, 19(3), 583–594.
- Manciu, M., & Ruckenstein, E. (2012). Ions near the air/water interface: I. Compatibility of zeta potential and surface tension experiments. *Colloids and Surfaces A: Physicochemical and Engineering Aspects*, 400, 27–35.
- Mane, S. P., Johnson, S. K., Duranti, M., Pareek, V. K., & Utikar, R. P. (2018). Lupin seed γ -conglutin: Extraction and purification methods-A review. *Trends in Food Science & Technology*, 73, 1–11.
- Martinez, K. D., Sanchez, C. C., Ruiz-Henestrosa, V. P., Patino, J. M. R., & Pilosof, A. M. (2007). Soy protein-polysaccharides interactions at the air-water interface. *Food Hydrocolloids*, 21(5–6), 804–812.
- McClements, D. J. (2006). Non-covalent interactions between proteins and polysaccharides. *Biotechnology Advances*, 24(6), 621–625.
- Munialo, C. D., van der Linden, E., Ako, K., & de Jongh, H. H. (2015). Quantitative analysis of the network structure that underlines the transitioning in mechanical responses of pea protein gels. *Food Hydrocolloids*, 49, 104–117.
- Perez, A. A., Carrara, C. R., Sánchez, C. C., Santiago, L. G., & Patino, J. M. R. (2009). Interfacial dynamic properties of whey protein concentrate/polysaccharide mixtures at neutral pH. *Food Hydrocolloids*, 23(5), 1253–1262.
- Perez, A. A., Carrara, C. R., Sánchez, C. C., Santiago, L. G., & Rodríguez Patino, J. M. (2010). Interfacial and foaming characteristics of milk whey protein and polysaccharide mixed systems. *AIChE Journal*, 56(4), 1107–1117.
- Pozani, S., Doxastakis, G., & Kiosseoglou, V. (2002). Functionality of lupin seed protein isolate in relation to its interfacial behaviour. *Food Hydrocolloids*, 16(3), 241–247.
- Raymundo, A., Empis, J., & Sousa, I. (1998). White lupin protein isolate as a foaming agent. *Zeitschrift für Lebensmittel-Untersuchung und -Forschung A*, 207, 91–96.
- Rodríguez-Ambriz, S., Martínez-Ayala, A., Millán, F., & Davila-Ortiz, G. (2005). Composition and functional properties of *Lupinus campestris* protein isolates. *Plant Foods for Human Nutrition*, 60, 99–107.
- Salmanowicz, B. P., & Weder, J. K. (1997). Primary structure of 2S albumin from seeds of *Lupinus albus*. *Zeitschrift für Lebensmittel-Untersuchung und -Forschung A*, 204, 129–135.
- Sarraf, M., Naji-Tabasi, S., & Beig-babaei, A. (2021). Influence of calcium chloride and pH on soluble complex of whey protein-basil seed gum and xanthan gum. *Food Science and Nutrition*, 9(12), 6728–6736.
- Sathe, S., Deshpande, S., & Salunkhe, D. (1982). Functional properties of lupin seed (*Lupinus mutabilis*) proteins and protein concentrates. *Journal of Food Science*, 47(2), 491–497.
- Shevkani, K., Singh, N., Chen, Y., Kaur, A., & Yu, L. (2019). Pulse proteins: Secondary structure, functionality and applications. *Journal of Food Science & Technology*, 56, 2787–2798.
- Shrestha, S., van't Hag, L., Haritos, V. S., & Dhital, S. (2021). Lupin proteins: Structure, isolation and application. *Trends in Food Science & Technology*, 116, 928–939.
- Stone, A. K., Cheung, L., Chang, C., & Nickerson, M. T. (2013). Formation and functionality of soluble and insoluble electrostatic complexes within mixtures of canola protein isolate and (κ -, ι - and λ -type) carrageenan. *Food Research International*, 54(1), 195–202.
- Takahashi, M. (2005). ζ potential of microbubbles in aqueous solutions: Electrical properties of the gas-water interface. *The Journal of Physical Chemistry B*, 109(46), 21858–21864.
- Tian, Y., Zhang, Z., Taha, A., Chen, Y., Hu, H., & Pan, S. (2020). Interfacial and emulsifying properties of β -conglycinin/pectin mixtures at the oil/water interface: Effect of pH. *Food Hydrocolloids*, 109, Article 106145.
- Xu, Y., Yang, N., Yang, J., Hu, J., Zhang, K., Nishinari, K., et al. (2020). Protein/polysaccharide intramolecular electrostatic complex as superior food-grade foaming agent. *Food Hydrocolloids*, 101, Article 105474.
- Yang, J., Berton-Carabin, C. C., Nikiforidis, C. V., van der Linden, E., & Sagis, L. M. (2022). Competition of rapeseed proteins and oleosomes for the air-water interface and its effect on the foaming properties of protein-oleosome mixtures. *Food Hydrocolloids*, 122, Article 107078.
- Yang, J., Thielen, I., Berton-Carabin, C. C., van der Linden, E., & Sagis, L. M. (2020). Nonlinear interfacial rheology and atomic force microscopy of air-water interfaces stabilized by whey protein beads and their constituents. *Food Hydrocolloids*, 101, Article 105466.
- Zhang, Q., Dong, H., Gao, J., Chen, L., & Vasanthan, T. (2020). Field pea protein isolate/chitosan complex coacervates: Formation and characterization. *Carbohydrate Polymers*, 250, Article 116925.
- Zhang, J., Du, H., Ma, N., Zhong, L., Ma, G., Pei, F., et al. (2023). Effect of ionic strength and mixing ratio on complex coacervation of soy protein isolate/Flammulina velutipes polysaccharide. *Food Science and Human Wellness*, 12(1), 183–191.